IEEE Access
Multidisciplinary | Rapid Review | Open Access Journal

Received October 22, 2018, accepted November 14, 2018, date of publication November 21, 2018,
date of current version December 27, 2018.

Digital Object Identifier 10.1109/ACCESS.2018.2882579

Maximum Likelihood Angle Estimation of Target in the Presence of Chaff Centroid Jamming

YEMIN LIU[1], SHIQI XING[1], YONGCAI LIU[1], YONGZHEN LI[1], AND XUESONG WANG[2]

[1]State Key Laboratory of Complex Electromagnetic Environment Effects on Electronics and Information System, National University of Defense Technology, Changsha 410073, China

[2]Graduate school, National University of Defense Technology, Changsha410073, China

Corresponding author: Yemin Liu (liuyemin2@163.com)

This work was supported by the National Natural Science Foundation of China under Grant 61490692.

ABSTRACT Chaff centroid jamming released by vessel causes the indicated angle of radar seeker of anti-ship missile to deviate from the target. The failure to track the target is catastrophic for the radar seeker. In this paper, the angle estimation of the target in the presence of chaff centroid jamming is investigated. In the circumstance of chaff centroid jamming, the jamming is usually in the same range and angle resolution cells as the target. Under these circumstances, the essence of this problem is to estimate two unresolved targets' angles in the main beam of the radar seeker. To this end, two alternative methods are proposed to estimate the direction of arrival of the target in this paper. First, we present a maximum likelihood (ML) method implemented by a 2-D numerical search, which has high estimation accuracy but large computational load. Subsequently, considering both the accuracy and computational load, an improved ML (IML) method is developed. Based on the ML method, the proposed IML method adopts a search optimization processing by moment estimation. Furthermore, the effects of some key factors on the estimation performance are analyzed. The accuracy of the proposed methods is compared with the existing methods and the Cramer Rao lower bound as well.

INDEX TERMS Monopulse radar, electronic counter-countermeasures, maximum likelihood estimator, direction of arrival (DOA), chaff centroid jamming.

I. INTRODUCTION

Chaff has been playing an important role in electronic warfare [1]. Releasing chaff centroid jamming is a common measure employed by a vessel when the vessel realizes the anti-ship missile has been tracking it [1], [2]. When the chaff centroid jamming is present, the indicated angle of radar seeker obtained by the in-phase monopulse ratio can wander far beyond the target and points to the centroid of the target and jamming [1]. If there are no effective countermeasures, the missile will eventually be induced by the chaff centroid jamming and miss the target. Therefore, the study on countermeasures against the chaff centroid jamming has significant value for the military.

The open literature on countermeasures against chaff centroid jamming can be typically divided into two research aspects. The first aspect is to detect the presence of chaff centroid jamming, and it is the premise and foundation for eliminating the catastrophic effect of the chaff centroid jamming. Based on the Neyman–Pearson algorithm, a detection method for chaff centroid jamming aided by Global Positioning System and Inertial Navigation System (GPS/INS) has been investigated by Yang *et al.* [2]. The second is to suppress the jamming or strengthen the target signal while suppressing the jamming, and then obtain the indicated angle by the traditional in-phase monopulse ratio. In this case, a typical approach is to use a polarization oblique projection to suppress the chaff centroid jamming of a radar seeker [3]. However, the sophisticated polarization system and the accurate priori polarization knowledge of the jamming are needed for the method proposed in [3].

In the circumstance of chaff centroid jamming, the chaff clouds must expand rapidly because it must present a cross section larger than the vessel while the vessel is still within the same resolution cell [1]. It is suggested that the vessel and jamming are two unresolved targets (i.e., occupying the same range and angle resolution cells) for the radar seeker, and the key to countermeasures against chaff centroid jamming is to estimate the angles of the vessel and jamming. The problem of angle estimation for two unresolved targets by utilizing a monopulse system has been addressed in several methods [4]–[11]. These methods fall into two categories: deterministic and statistical. Deterministic methods generally

use one or two pulses to estimate angle and are not restricted by the target model [4]. Sherman used two consecutive pulses to estimate the angles of two nonfluctuating or slowly fluctuating targets which are in the same resolution cell [5]. Afterward, Lee et al. presented an important improvement on Sherman's method by using an algebraic method [4]. However, the fast fluctuating targets (e.g., Swerling IV targets) may limit the use of the approaches in [4] and [5]. Zheng *et al.* [6] presented a closed-form solution for the angles of arrival of returns from two unresolved targets, and aiming at the proposed method in [6], a mathematically equivalent algorithm that has a marginally lower computational complexity has been presented by Crouse *et al.* [7]. It is worth noting that, if the elevation angles of the two targets are nearly equal, the azimuth angle estimates have large variances for the proposed methods in [6] and [7]. For chaff centroid jamming, elevation angles of the target and jamming are the same in most cases [1], [2]. In this condition, the proposed methods in [6] and [7] may be ineffective.

The statistical methods may achieve a more accurate solution than deterministic methods, because this technique generally uses multiple pulses [4]. Vincent *et al.* [8] presented an approximate unconditional maximum likelihood (ML) direction of arrival (DOA) estimation method for two unresolved targets. However, considering the limitation of space of the platform itself, the antenna configuration of a uniform linear array in [8] may not be suitable for the anti-ship missile. In addition, Blair and Brandt-Pearce [9] used the statistics of the in-phase and quadrature monopulse ratios to develop a DOA estimation method for two unresolved Rayleigh (Swerling I) targets. Sinha *et al.* [10] presented the numerical ML estimator for both Swerling I and Swerling III models. Subsequently, the ML computation has been made explicit for two unresolved Swerling I targets by Wang *et al.* [11]. However, the statistical methods stated above may not be an optimal estimator for countering the chaff centroid jamming by radar seeker. Because the targets considered in [8]–[11] are all the same targets (i.e., both Swerling I or Swerling III targets), whereas the radar seeker is more likely to be faced with two different types of targets [2]. The study on the angle estimation methods for the two different types of unresolved targets in a standard monopulse radar has not been reported in the open literature. So, this paper is the initial trial to fill this knowledge vacancy. In addition, some literature [12]–[14] proposed the use of wideband monopulse radar to estimate the angle of a target (i.e., extended target). This monopulse radar may or may not eventually become the standard, but in the present day many radars use traditional monopulse [11]. Therefore, we consider narrowband monopulse radar, and suppose that the target and jamming are point targets.

The rest of this paper is organized as follows. In Section II, the problem is formulated, and the statistical properties of the vessel and chaff are reviewed. In Section III, the maximum likelihood estimator in the presence of chaff centroid jamming is derived, and the numerical calculation method of the Cramer Rao lower bound (CRLB) is presented. In Section IV,

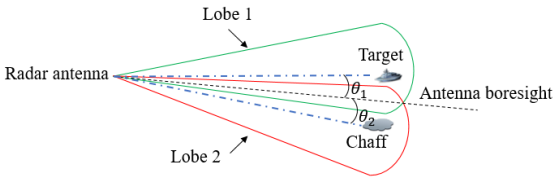

FIGURE 1. Diagram of the chaff centroid jamming for an amplitude comparison monopulse system.

an improved maximum likelihood (IML) method is proposed. The search optimization processing and computational complexity analysis of the IML method are presented. In Section V, the influences of some key factors on the DOA estimation of the target are analyzed. The accuracy of the proposed methods is compared with the existing methods and the CRLB by the Monte Carlo trials. The conclusions are drawn in Section VI.

II. MODEL

In a typical amplitude comparison monopulse radar, the radar uses four squinted sub-beams to estimate the target azimuth and elevation angles. For the chaff centroid jamming, elevation angles of the target and jamming are usually the same, angle difference mainly exists in azimuth [1], [2]. Hence, we will mainly consider the estimation of target azimuth angle in this paper.

When the chaff centroid jamming is present, the target and jamming are in the same range and angle resolution cells, shown in Fig. 1. Then, at time t, the sum and difference signals can be expressed as follows [15]

$$\begin{aligned} S(t) &= \sum_{j=1}^{2} \sqrt{\kappa} A_i G_{\sum}^2 \left(\theta_j\right) p(t) \cos\left(\omega_c t - \phi_j\right) + N_S(t) \\ D(t) &= \sum_{j=1}^{2} \eta_j \sqrt{\kappa} A_i p(t) \cos\left(\omega_c t - \phi_j\right) + N_D(t) \end{aligned} \tag{1}$$

where S refers to sum signal, and D denotes difference signal. N_S and N_D indicate the receiver noises in the sum and difference channel, respectively. κ is constant proportional to transmitted power. A_1 and A_2 are voltage amplitudes of the target and jamming, respectively. $G_{\sum}\left(\theta_j\right)$ is the sum channel voltage gain at angle θ_j $(j = 1, 2)$. θ_1 and θ_2 are the off-boresight angles of the target and jamming, respectively. η_1 and η_2 are the DOAs of the target and jamming, respectively. $p(t)$ is the envelope of transmitted pulse, and ω_c is the carrier frequency (in radians per second) of transmitted pulse. ϕ_1 and ϕ_2 are the phases of the vessel and jamming, respectively.

The sum and difference signals are demodulated and passed through the matched filter. Then, the in-phase and quadrature components of the sum and difference channel can be given by [10], [15]

$$\begin{aligned} s_I &= \alpha_1 \cos\phi_1 + \alpha_2 \cos\phi_2 + n_{sI} \\ s_Q &= \alpha_1 \sin\phi_1 + \alpha_2 \sin\phi_2 + n_{sQ} \\ d_I &= \eta_1\alpha_1 \cos\phi_1 + \eta_2\alpha_2 \cos\phi_2 + n_{dI} \\ d_Q &= \eta_1\alpha_1 \sin\phi_1 + \eta_2\alpha_2 \sin\phi_2 + n_{dQ} \end{aligned} \tag{2}$$

where s refers to the sum signals, d denotes the difference signals, and n indicates the receiver noises. The subscripts I and Q represent the in-phase and quadrature components, respectively. $\alpha_j = \sqrt{\kappa} A_i G_{\sum}^2(\theta_j) p_0$, p_0 is the receiver matched filter gain.

When denoting $\alpha_j \cos\phi_j$ by x_j and $\alpha_j \sin\phi_j$ by y_j (in-phase and quadrature signal components), it leads to

$$\begin{aligned} s_I &= x_1 + x_2 + n_{sI} \\ s_Q &= y_1 + y_2 + n_{sQ} \\ d_I &= \eta_1 x_1 + \eta_2 x_2 + n_{dI} \\ d_Q &= \eta_1 y_1 + \eta_2 y_2 + n_{dQ} \end{aligned} \tag{3}$$

where the random variables x_1 and y_1 are the returns from the vessel, and x_2 and y_2 are from the jamming. For a standard amplitude comparison monopulse system, the relationship between the DOA and the angle θ_j can be approximately given by $\eta_j = k_m \theta_j$ within one-half of a beamwidth of antenna boresight, where k_m denotes the average error slope [16]. Since it is easy to obtain the DOA η_j by the angle θ_j, here we only consider the DOA estimates.

In this paper, the receiver noises including the sea clutter and the thermal noise will be seen as Gauss white noises with zero mean [2]. This assumption can be justified by the following argument: in a monopulse radar system, there are many situations where the clutter (e.g., ground or sea clutter) can be removed by the signal processing methods along the range of the target [5]. Following [5], [9]–[11], [15], [16], and many others, here, we assume that the Gauss white noises of in-phase and quadrature components of the sum and difference channel are independent with each other, and with known variances, which can be estimated reasonably well [11]

$$\begin{aligned} \mathrm{Var}[n_{sI}] &= \mathrm{Var}[n_{sQ}] = \sigma_s^2 \\ \mathrm{Var}[n_{dI}] &= \mathrm{Var}[n_{dQ}] = \sigma_d^2 \end{aligned} \tag{4}$$

where $\mathrm{Var}(\cdot)$ is stand for variance operation.

Assuming that radar cross-section (RCS) of the vessel obeys Swerling IV model [2], with uniformly distributed phase ϕ_1 within $[0, 2\pi]$ [9]–[11], the probability density function (PDF) of x_1 can be expressed as [10]

$$p(x_1) = \frac{4}{\sqrt{2\pi} a_1^3} \left(x_1^2 + \frac{a_1^2}{4} \right) \exp\left(-\frac{2x_1}{a_1^2} \right) \tag{5}$$

where, $E(x_1^2) = a_1^2/2$, $a_1^2 = E(\alpha_1^2)$, $E(\cdot)$ denotes the expected value. Further, considering that the RCS of the chaff clouds obeys the Swerling II model [2], similarly, the PDF of x_2 can be written as

$$p(x_2) = \frac{1}{\sqrt{2\pi a_2^2}} \exp\left(-\frac{x_2}{2a_2^2} \right) \tag{6}$$

where $E(x_2^2) = a_2^2$, $a_2^2 = E(\alpha_2^2)/2$. Furthermore, for quadrature components, y_1 and y_2 have the same PDFs as x_1 and x_2, respectively.

III. MAXIMUM LIKELIHOOD ESTIMATOR IN THE PRESENCE OF CHAFF CENTROID JAMMING

A. DERIVATION OF LIKELIHOOD FUNCTION

Using the statistical characteristics of the observation model in Section II, the two DOA estimates of the target and jamming are obtained by maximizing the corresponding likelihood function

$$[\hat{\eta}_1, \hat{\eta}_2] = \arg\max_{\eta_1, \eta_2} \{L(\eta_1, \eta_2)\} \tag{7}$$

where

$$L(\eta_1, \eta_2) = p(s_I, s_Q, d_I, d_Q | \eta_1, \eta_2) \tag{8}$$

In (8), considering that the independence of the in-phase and quadrature channels [11], the likelihood function $L(\eta_1, \eta_2)$ can be written as

$$\begin{aligned} L(\eta_1, \eta_2) &= L_I(\eta_1, \eta_2) \times L_Q(\eta_1, \eta_2) \\ &= p(s_I, d_I | \eta_1, \eta_2) \times p(s_Q, d_Q | \eta_1, \eta_2) \end{aligned} \tag{9}$$

Substituting (3), (4), (5) and (6) into (9), then we can obtain the function $L_I(\eta_1, \eta_2)$ of η_1 and η_2 as

$$\begin{aligned} &L_I(\eta_1, \eta_2) \\ &= \frac{4}{2\pi a_1^3 a_2 \sqrt{b_1 b_2 - l^2}} \exp\left[-\frac{1}{2R} \left(s_I^2 \sigma_d^2 + d_I^2 \sigma_s^2 \right) \right] \\ &\quad \times \exp\left[\frac{c_1^2 b_2 + c_2^2 b_1 - 2c_1 c_2 l}{2R(b_1 b_2 - l^2)} \right] \\ &\quad \times \left(f_1^I(\eta_1, \eta_2) + f_2^I(\eta_1, \eta_2) \right) \end{aligned} \tag{10}$$

where

$$\begin{aligned} R &= \sigma_s^2 \sigma_d^2 \\ b_1 &= \sigma_d^2 + \eta_1^2 \sigma_s^2 + 4\sigma_s^2 \sigma_d^2 / a_1^2 \\ b_2 &= \sigma_d^2 + \eta_2^2 \sigma_s^2 + \sigma_s^2 \sigma_d^2 / a_2^2 \\ c_1 &= s_I \sigma_d^2 + \eta_1 d_I \sigma_s^2 \\ c_2 &= s_I \sigma_d^2 + \eta_2 d_I \sigma_s^2 \\ l &= \sigma_d^2 + \eta_1 \eta_2 \sigma_s^2 \end{aligned} \tag{11}$$

$$f_1^I(\eta_1, \eta_2) = \frac{l^2}{b_1^2} \left(\sigma_{x_2}^2 + \mu_{x_2}^I \right) + \frac{a_1^2}{4}$$

$$f_2^I(\eta_1, \eta_2) = \frac{c_1^2}{b_1^2} + \frac{R}{b_1} - \frac{2c_1 l}{b_1} \mu_{x_2}^I \tag{12}$$

$$\begin{aligned} \sigma_{x_2}^2 &= \frac{R b_1}{b_1 b_2 - l^2} \\ \mu_{x_2}^I &= \frac{c_2 b_1 - c_1 l}{b_1 b_2 - l^2} \end{aligned} \tag{13}$$

A detailed derivation is available in Appendix. In addition, the function $L_Q(\eta_1, \eta_2)$ (see (51) in Appendix) has similar PDF with $L_I(\eta_1, \eta_2)$.

For two unresolved Swerling I targets, the ML method proposed in [10] has been made explicit by Wang *et al.* [11]. However, for unresolved Swerling IV and Swerling II targets (i.e., mixed targets), no closed-form solutions for the likelihood function in (9) are available, and one feasible method is

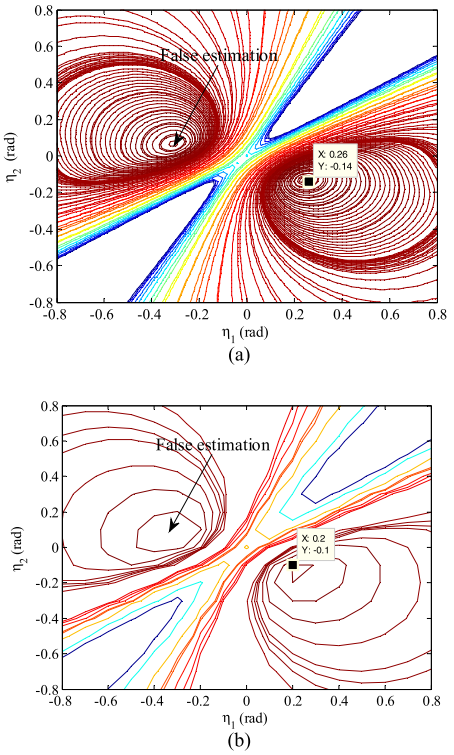

FIGURE 2. Contour plot of the log-likelihood function of η_1 and η_2 for different search steps. (a) Search step is 0.02 rad, and the DOA estimation of the target is 0.26 rad; (b) Search step is 0.1 rad, and the DOA estimation of the target is 0.2 rad.

to use a grid search to find estimates of η_1 and η_2 [10]. The typical contour plot of the log-likelihood function of η_1 and η_2 of two targets is shown in Fig. 2, for 25 dB signal-to-noise ratio (SNR) of the target and -4 dB signal-to-interference ratio (SIR). The actual values of η_1 and η_2 are 0.25 and -0.15 rad, respectively. In Fig. 2, there are two maximum estimations due to the uncertainty of the relative size of η_1 and η_2 [10]. Thus, we need to reject the false one using prior knowledge (i.e., relative size of η_1 and η_2), and this prior knowledge can be obtained by the method in [2].

It is worth noting that, for the grid search method, if the grid partition of the search is very accurate, there will be a large computational load, which is not practical for real-time processing. Otherwise, the estimation accuracy of the target's DOA will be decreased. For instance, in Fig. 2, the simulation parameters in Fig. 2 (a) and Fig. 2 (b) are the same, except that the search steps in Fig. 2 (a) and Fig. 2 (b) are 0.02 and 0.1 rad, respectively. It is found that the estimation error of the target's DOA in Fig. 2 (a) is small but the computational load on search is larger than that in Fig. 2 (b), while the DOA of the target has a greater error in Fig. 2 (b) than that in Fig. 2 (a) due to the low grid accuracy. To analyze quantitatively the effect of the grid layout on the DOA estimation of the target, the relationship between the root mean square error (RMSE) of η_1 estimation and the search step is shown in Fig. 3. For different search steps (i.e., 0.01, 0.05, 0.1, 0.15 and 0.2 rad), the RMSE of η_1 estimation is calculated by 5000 Monte Carlo

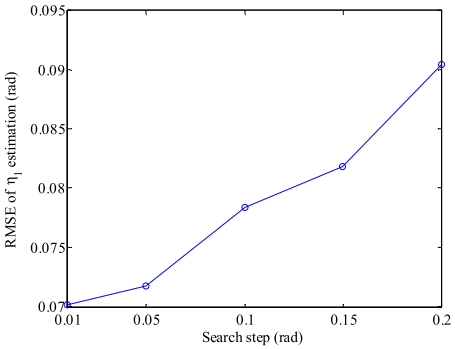

FIGURE 3. Relationship between the RMSE of η_1 estimation and the search step.

trials in Fig. 3. It is clear that the higher the grid accuracy is, the smaller the RMSE (i.e., better estimation accuracy) is. Therefore, when the high estimation accuracy is required, we need to consider the grid partition.

B. CRLB OF DOA ESTIMATION

The likelihood function in (9) for two unresolved mixed targets are infinite polynomials of s_I, d_I, s_Q and d_Q. Thus, the closed-form solutions for the calculation of the CRLB are not available. However, the CRLB can be obtained by evaluating the expectation numerically using the law of large numbers [10]. To this end, taking the logarithm in (9), the Fisher information matrix (FIM) for DOA estimates can be given by

$$J \cong E\left\{\left[\nabla_\eta \log\left(L\left(\eta_1, \eta_2\right)\right)\right]^{\mathrm{T}}\left[\nabla_\eta \log\left(L\left(\eta_1, \eta_2\right)\right)\right]\right\} \quad (14)$$

where, the operation $\cong$ indicates that the left terms are estimated by the expressions on the right. The symbol T and ∇ denote transpose and gradient operation, respectively.

Using the law of large numbers, it leads to

$$J \cong \frac{1}{M}\sum_{m=1}^{M}\left[\nabla_\eta \log\left(L\left(\eta_1, \eta_2\right)\right)\right]_m^{\mathrm{T}}\left[\nabla_\eta \log\left(L\left(\eta_1, \eta_2\right)\right)\right]_m \quad (15)$$

where the subscript m means the value of the gradient obtained in the mth realization, i.e., for the mth set of values of s_I, d_I, s_Q and d_Q. The larger M is, the closer the result in (15) is to the theoretical FIM in (14).

Furthermore, if N subpulses at distinct frequencies are used (i.e., s_I, d_I, s_Q and d_Q are independent with each other [9]), the FIM for η_1 and η_2 estimates is then given by

$$J_N = NJ \quad (16)$$

When inversing of the matrix J_N in (16), the CRLB of η_1 and η_2 is obtained finally.

IV. IMPROVED MAXIMUM LIKELIHOOD METHOD

From Section III (A), the ML method has the contradiction between estimation accuracy and real-time performance due to its two dimensional numerical search. To solve this contradiction, in this section, we develop an IML method that is

efficient in accuracy and computational load. Based on the ML method, the IML method adopts a search optimization processing. The relationship between η_1 and η_2 is deduced by moment estimation, which transforms the two-dimensional numerical search into one-dimensional numerical search, thus improving the computational efficiency. The processing in detail is as follows.

A. SEARCH OPTIMIZATION PROCESSING

Based on the observation model in Section II, it is reasonable to assume that x_1, x_2 and n_{sI} are independent with each other. According to (4), (5) and (6), we can obtain the second-moment of the in-phase component of the sum channel s_I

$$E\left(s_I^2\right) = a_1^2/2 + a_2^2 + \sigma_s^2 \tag{17}$$

Similarly, we can also obtain the second-moment of the in-phase component of the difference channel d_I

$$E\left(d_I^2\right) = \eta_1^2 a_1^2/2 + \eta_2^2 a_2^2 + \sigma_d^2 \tag{18}$$

From Section II, it is noted that s_Q has the same PDF as s_I and d_Q has the same PDF as d_I. Therefore, the second-moment of s_Q and d_Q are the same as (17) and (18), respectively. Moreover, the second-moment of the in-phase component of the sum and difference channel can be expressed as

$$E\left(s_I d_I\right) = \eta_1 a_1^2/2 + \eta_2 a_2^2 \tag{19}$$

For N subpluses at distinct frequencies, on the other hand, the second-moments in (17), (18) and (19) can be estimated as

$$\begin{aligned} E\left(s_I^2\right) = E\left(s_Q^2\right) &\cong \frac{1}{2N}\sum_{i=1}^{N}\left\{s_I^2(i) + s_Q^2(i)\right\} \\ &= \frac{B_2 + 2N\sigma_s^2}{2N} \end{aligned} \tag{20}$$

$$\begin{aligned} E\left(s_I d_I\right) = E\left(s_Q d_Q\right) &\cong \frac{1}{2N}\sum_{i=1}^{N}\left\{s_I(i)\, d_I(i) + s_Q(i)\, d_Q(i)\right\} \\ &= \frac{B_1}{2N} \end{aligned} \tag{21}$$

$$\begin{aligned} E\left(d_I^2\right) = E\left(d_Q^2\right) &\cong \frac{1}{2N}\sum_{i=1}^{N}\left\{d_I^2(i) + d_Q^2(i)\right\} \\ &= \frac{B_0 + 2N\sigma_d^2}{2N} \end{aligned} \tag{22}$$

where the definitions of B_2, B_1 and B_0 are

$$\begin{aligned} B_2 &= \sum_{i=1}^{N}\left\{s_I^2(i) + s_Q^2(i)\right\} - 2N\sigma_s^2 \\ B_1 &= \sum_{i=1}^{N}\left\{s_I(i)\, d_I(i) + s_Q(i)\, d_Q(i)\right\} \\ B_0 &= \sum_{i=1}^{N}\left\{d_I^2(i) + d_Q^2(i)\right\} - 2N\sigma_d^2 \end{aligned} \tag{23}$$

According to (17), (19), (20) and (21), a_1^2 and a_2^2 can be expressed in matrix form

$$\begin{bmatrix} 1/2 & 1 \\ \eta_1/2 & \eta_2 \end{bmatrix}\begin{bmatrix} a_1^2 \\ a_2^2 \end{bmatrix} = \begin{bmatrix} B_2/(2N) \\ B_1/(2N) \end{bmatrix} \tag{24}$$

In (24), applying Cramer's rule [17], we have

$$a_1^2 = \frac{B_2\eta_2 - B_1}{N(\eta_2 - \eta_1)} \tag{25}$$

$$a_2^2 = \frac{B_1 - B_2\eta_1}{2N(\eta_2 - \eta_1)} \tag{26}$$

Similarly, according to (17), (18), (20) and (22), a_1^2 and a_2^2 can be written as

$$a_1^2 = \frac{B_1\eta_2 - B_0}{\eta_1 N(\eta_2 - \eta_1)} \tag{27}$$

$$a_2^2 = \frac{B_0 - B_1\eta_1}{2\eta_2 N(\eta_2 - \eta_1)} \tag{28}$$

Combining (25) and (27), we get

$$\eta_1 = g(\eta_2) = \frac{B_1\eta_2 - B_0}{B_2\eta_2 - B_1} \tag{29}$$

According to (26) and (28), we have

$$\eta_2 = g(\eta_1) = \frac{B_1\eta_1 - B_0}{B_2\eta_1 - B_1} \tag{30}$$

Equations (29) and (30) are equivalent and can be expressed for each other. In (29) and (30), it is found that the relationship (i.e., η_1 and η_2) can be revealed through estimating the second-moment of the signal echoes. Therefore, based on the ML method, we can reduce the two-dimensional likelihood function (9) into one dimension (only including variable η_1) by (30). In other words, based on the ML method, the IML method optimizes the search algorithm by second-moment estimation, and this is the main idea for the IML method. Then, for N subpulses at distinct frequencies, we have the overall log-likelihood function of η_1

$$\begin{aligned} \hat{\eta}_1 &= \arg\max_{\eta_1}\left\{\sum_{i=1}^{N}\log\tilde{L}^i(\eta_1)\right\} \\ &= \arg\max_{\eta_1}\left\{\sum_{i=1}^{N}\log\tilde{L}_I^i(\eta_1) + \sum_{i=1}^{N}\log\tilde{L}_Q^i(\eta_1)\right\} \end{aligned} \tag{31}$$

where

$$\begin{aligned} \tilde{L}_I^i(\eta_1) = &\frac{4}{2\pi a_1^3 a_2\sqrt{b_1\tilde{b}_2 - \tilde{l}^2}} \\ &\times \exp\left[-\frac{1}{2R}\left(s_I^2(i)\sigma_d^2 + d_I^2(i)\sigma_s^2\right)\right] \\ &\times \exp\left[\frac{c_1^2\tilde{b}_2 + \tilde{c}_2^2 b_1 - 2c_1\tilde{c}_2\tilde{l}}{2R\left(b_1\tilde{b}_2 - \tilde{l}^2\right)}\right] \\ &\times \left(\tilde{f}_1^I(\eta_1) + \tilde{f}_2^I(\eta_1)\right) \\ \tilde{L}_Q^i(\eta_1) = &\frac{4}{2\pi a_1^3 a_2\sqrt{b_1\tilde{b}_2 - \tilde{l}^2}} \end{aligned}$$

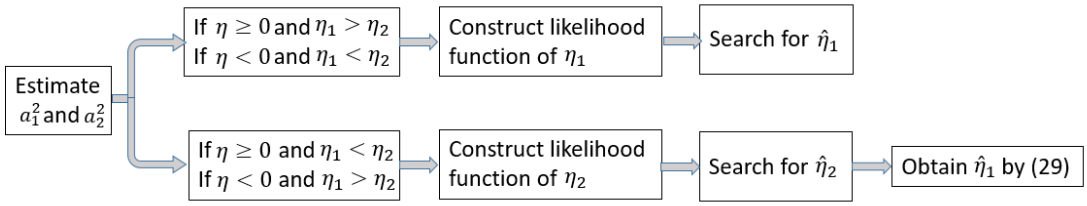

FIGURE 4. Flowchart of the DOA estimation of target for the IML method.

$$\times \exp\left[-\frac{1}{2R}\left(s_Q^2(i)\sigma_d^2 + d_Q^2(i)\sigma_s^2\right)\right] \times \exp\left[\frac{d_1^2\tilde{b}_2 + \tilde{d}_2^2 b_1 - 2d_1\tilde{d}_2\tilde{l}}{2R\left(b_1\tilde{b}_2 - \tilde{l}^2\right)}\right] \times \left(\tilde{f}_1^Q(\eta_1) + \tilde{f}_2^Q(\eta_1)\right) \tag{32}$$

and

$$\begin{aligned} \tilde{b}_2 &= \sigma_d^2 + g^2(\eta_1)\sigma_s^2 + \sigma_s^2\sigma_d^2/a_2^2 \\ \tilde{c}_2 &= s_I(i)\sigma_d^2 + g(\eta_1)d_I(i)\sigma_s^2 \\ \tilde{d}_2 &= s_Q(i)\sigma_d^2 + g(\eta_1)d_Q(i)\sigma_s^2 \\ \tilde{l} &= \sigma_d^2 + \eta_1 g(\eta_1)\sigma_s^2 \end{aligned} \tag{33}$$

$$\begin{aligned} \tilde{f}_1^I(k_1) &= \frac{\tilde{l}^2}{b_1^2}\left(\tilde{\sigma}_{x_2}^2 + \tilde{\mu}_{x_2}^I\right) + \frac{a_1^2}{4} \\ \tilde{f}_2^I(k_1) &= \frac{c_1^2}{b_1^2} + \frac{R}{b_1} - \frac{2c_1 l}{b_1}\tilde{\mu}_{x_2}^I \\ \tilde{f}_1^Q(k_1) &= \frac{\tilde{l}^2}{b_1^2}\left(\tilde{\sigma}_{x_2}^2 + \tilde{\mu}_{x_2}^Q\right) + \frac{a_1^2}{4} \\ \tilde{f}_2^Q(k_1) &= \frac{c_1^2}{b_1^2} + \frac{R}{b_1} - \frac{2c_1 l}{b_1}\tilde{\mu}_{x_2}^Q \end{aligned} \tag{34}$$

$$\begin{aligned} \tilde{\sigma}_{x_2}^2 &= \frac{R\tilde{b}_1}{b_1\tilde{b}_2 - l^2} \\ \tilde{\mu}_{x_2}^I &= \frac{\tilde{c}_2 b_1 - c_1\tilde{l}}{b_1\tilde{b}_2 - \tilde{l}^2} \\ \tilde{\mu}_{x_2}^Q &= \frac{\tilde{d}_2 b_1 - d_1\tilde{l}}{b_1\tilde{b}_2 - \tilde{l}^2} \end{aligned} \tag{35}$$

Similarly, if necessary, we can first obtain the likelihood function of η_2 and then get η_1 according to (29).

Moreover, in our implementations, we estimate a_1^2 and a_2^2 from the observed signal echoes with a known value of the relative radar cross section (RRCS) γ [9]–[11].

$$\begin{aligned} \hat{a}_1^2 &= \frac{2}{1+\gamma}\left(\frac{1}{2N}\sum_{i=1}^{N}\left\{s_I^2(i) + s_Q^2(i)\right\} - \sigma_s^2\right) \\ \hat{a}_2^2 &= \frac{\gamma}{1+\gamma}\left(\frac{1}{2N}\sum_{i=1}^{N}\left\{s_I^2(i) + s_Q^2(i)\right\} - \sigma_s^2\right) \end{aligned} \tag{36}$$

where

$$\gamma = \frac{E\left(\alpha_2^2\right)}{E\left(\alpha_1^2\right)} = \frac{2a_2^2}{a_1^2} \tag{37}$$

Discussions above have presented the key procedures to estimation the target's DOA in the IML method (as shown in Fig. 4). Now, it is appropriate to make a summary of the main workflow in the following steps.

Step 1. Estimate a_1^2 and a_2^2 from the observed signal echoes.

Step 2. Calculate the DOA estimate of in-phase monopulse ratio $\eta = A_1/A_2$, and determine the relative size of the values of η_1 and η_2. The priori information of the relationship between η_1 and η_2 can be obtained by the method in [2].

Step 3. Construct likelihood function. We obtain the relationship between η_1 and η_2 through estimating the second-moment of the signal echoes. If $\eta \geq 0$ and $\eta_1 > \eta_2$ (maybe $\eta < 0$ and $\eta_1 < \eta_2$), the likelihood function of η_1 is constructed. In other cases, we construct the likelihood function of η_2.

Step 4. Search for $\hat{\eta}_1$. Especially, when the likelihood function of η_2 is constructed, we first search for $\hat{\eta}_2$, and then obtain the $\hat{\eta}_1$ by (29).

B. COMPUTATIONAL COMPLEXITY ANALYSIS

Recall that the likelihood function (9), the maximization of (9) is performed by a two-dimensional grid search on the portion of the $\eta_1 - \eta_2$ plane that agrees with the prior information. To compare the computational complexity of the ML and IML methods, without loss of generality, suppose that the expected value of $\eta_1 > \eta_2$ is known. To this end, for each $\eta_j s$ $(j = 1, 2)$, it is further assumed the search interval is divided into M equal parts (i.e., the number of grid partitions is M). For the ML method, we perform the search in that portion of $\eta_1 - \eta_2$ plane where $\eta_1 - \eta_2 > 0$ [10], and need to search $M(M-1)/2$ times to obtain $\hat{\eta}_1$. While for the IML method, if $\eta \geq 0$, we only need to search for $\hat{\eta}_1$ in the interval $[\eta, \eta_{bw}]$, where η_{bw} denotes the one-way, half-power DOA point on the antenna gain pattern in the sum channel [9]. If $\eta < 0$, first of all, we search for $\hat{\eta}_2$ in the interval $[-\eta_{bw}, \eta]$, then, we can acquire $\hat{\eta}_1$ by (29). Perhaps the worst case is $\eta = 0$, and if so, we need to search $floor\left((M-1)/2\right)$ times, where the operator $floor(\cdot)$ denotes round down. It is assumed that η is uniformly distributed over the interval $[-\eta_{bw}, \eta_{bw}]$. In this case, the average search is $floor\left((M-1)/4\right)$ times for acquiring $\hat{\eta}_1$. Therefore,

TABLE 1. Comparison of computational complexity of the ML and IML methods.

	η_{bw} (rad)	Search step (rad)	Grid partitions	Worst search (times)	Average search (times)
IML	0.8	0.01	161	80	40
ML	0.8	0.01	161	12880	12880

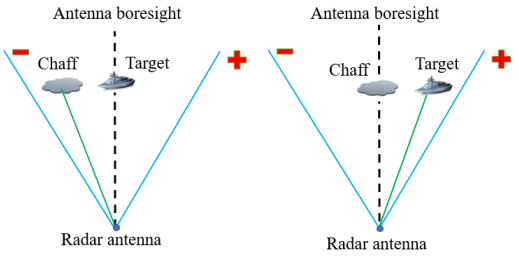

FIGURE 5. Sketch map of the relative position of the target and jamming.

compared with the ML method, the average search of the IML method is reduced by $2M$ times. The comparison results of computational complexity of the ML and IML methods are shown in Table 1. Obviously, the worst search need only 80 times in the IML method, which effectively improves the computation efficiency.

V. SIMULATION RESULTS

In this section, we first compare the estimation performance of the ML and IML methods discussed in the Section III (A) and Section IV. In the simulation, 5000 Monte Carlo trials are carried out, and the antenna gain issue is omitted for simplicity. The values $\sigma_s^2 = 1$ and $\sigma_d^2 = 1$ are used. For a typical monopulse system, the average error slope k_m in beamwidths is $k_m \approx 2\eta_{bw}$ [9]. So, for all the cases in this work, let $\eta_{bw} = 0.8$ rad [9]. For a set of positions of the target regarding the antenna boresight of the radar beam, the RMSE of DOA estimate of the target is calculated. We set $\eta_1 - \eta_2 = 0.4$ and the step rate of η_1 is 0.038 rad. The simulation starts with the target on one side of the antenna boresight ($\eta_1 = 0$ rad or $\eta_2 = -0.4$ rad) and ends the jamming on the other side of the antenna boresight ($\eta_1 = 0.4$ rad or $\eta_2 = 0$ rad). The sketch map of the relative position of the target and jamming in the simulation experiment is shown in Fig. 5. If $\eta_1 = 0.2$ rad, this would imply that the target and jamming symmetrically placed in the antenna boresight.

The RMSE of the estimation of the target's DOA for different values of the number of subpluses N, SNR and SIR is studied. The notation ML refers to the method discussed in Section III (A), IML to Section IV, and Square root of CRLB to the computational method introduced in Section III (B). The search step is 0.01 rad in the ML and IML methods. The RMSE of η_1 estimation for different values of N is shown in Fig. 6. For each N, let SNR = 20 dB, SIR = -4 dB. In Fig. 6 (a), it is noted that the efficiency

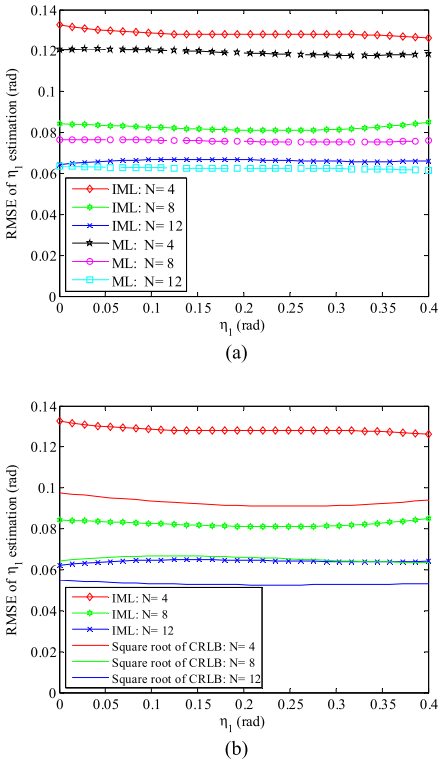

FIGURE 6. The estimation performance of the target's DOA for different values of *N*. (a) Given different *N*, RMSE in the estimation of the target's DOA for SNR = 20 dB and SIR = −4 dB; (b) RMSE in the estimation of the target's DOA versus square root of CRLB.

of each DOA estimate generally improves (i.e., the RMSE is getting smaller) as the number of subpulses N increases from 4 to 12. The RMSE of the two methods remains almost constant over the range of η_1, and the RMSE of IML has slightly higher value than that of ML in conditions of the same number of subpulses N. Specifically, as the number of subpulses N increases, the estimation performance of IML is more and more close to ML. In Fig. 6 (b), the RMSE of η_1 estimated by the IML algorithm is compared to the square root of the CRLB, and the CRLB is obtained by the result of 1000 realizations. It can be seen from Fig. 6 (b) that the accuracy of the DOA estimation improves when increasing the number of subpulses N at distinct frequencies in a radar pulse.

The RMSE of η_1 estimation versus square root of the CRLB as a funciton of SNR is studied. Here we assume SIR = -4 dB, and $N = 8$. The RMSE versus square root of the

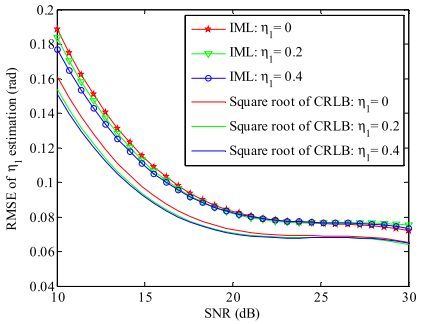

FIGURE 7. RMSE of the estimation of the target's DOA versus the square root of the CRLB as a function of SNR.

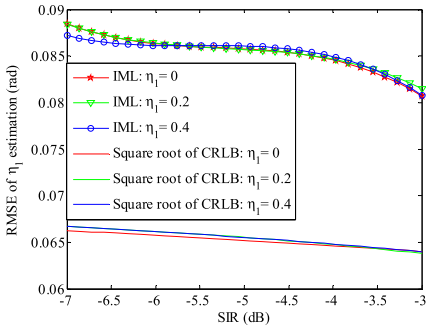

FIGURE 8. RMSE of the estimation of the target's DOA versus the square root of the CRLB as a function of SIR.

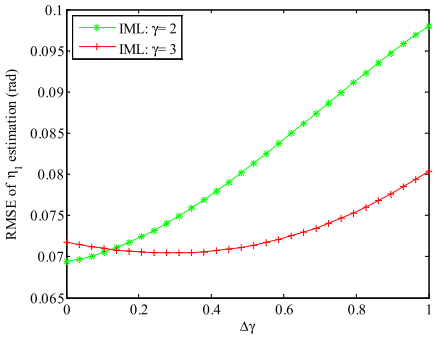

FIGURE 9. Relationship between the RMSE of η_1 estimation and the parameter $\Delta\gamma$.

CRLB is investigated when choosing different values of η_1 in Fig. 7. When $\eta_1 = 0$ rad, the antenna boresight is pointed at the target. Similarly, when $\eta_1 = 0.2$ rad, the antenna boresight is pointed at the middle of the target and jamming, and the antenna boresight is pointed at the jamming for $\eta_1 = 0.4$ rad. It is observed that the IML method offers almost the same estimation performance for different η_1, and the RMSE of η_1 estimation is more and more close to the square root of the CRLB as the SNR increases. In addition, it is also noted that the estimation performance of η_1 has been improved considerably when SNR $>$ 20 dB. For anti-ship applications, according to the scattering coefficient of the sea surface in [18], it can be calculated that the SNR of a given vessel is usually greater than 20 dB under the three-level sea state [2], [19]. Under this circumstance, the RMSE of η_1 estimation is less than 0.083 for the IML method in Fig. 7.

The effect of SIR on DOA estimation is also studied. For $N = 8$, SNR $= 20$ dB and different values of η_1 (i.e., $\eta_1 =$ 0, 0.2 and 0.4 rad), the RMSE of η_1 estimated by the IML methods and the square root of the CRLB are shown in Fig. 8. In the given range of SIR (i.e. [-7 dB, -3 dB]), it is shown in Fig. 8 that the RMSE and the square root of the CRLB have a slight improvement with the increase of SIR. For instance, when $\eta_1 = 0.2$ rad, the RMSE of η_1 estimation for SIR $=$ -3 dB is only improved by 0.006 than that for SIR $= -7$ dB. Thus, compared with the number of subpulses N and SNR, SIR has little effect on the estimation of the target's DOA.

According to the previous theoretical analysis, the actual RRCS γ is assumed to be known. This is an ideal situation, and it serves as a performance bound with the reality. Therefore, in the following, the effect of γ estimation on the RMSE of η_1 estimation is quantitatively analyzed. In the circumstance of chaff centroid jamming, for the anti-ship missile, the RCS of the chaff clouds is generally $2 \sim 3$ times that of the vessel [1], [2]. So, in the simulation experiment, the range of the RRCS can be set $\gamma \in [2, 3]$ (i.e., SIR $\in$ [-4.8 dB, -3 dB]). Suppose that the estimated RRCS is γ_e, and let $\Delta\gamma = |\gamma - \gamma_e|$. Then, when $\gamma_e \in [2, 3]$, we have $\Delta\gamma \in [0, 1]$. The relationship between the RMSE of η_1 estimation and the parameter $\Delta\gamma$ is shown in Fig. 9, for $N = 8$, SNR $= 25$ dB and $\eta_1 = 0.2$ rad. From Fig. 9, it is observed that the RMSE of η_1 estimation for $\gamma = 2$ (i.e., SIR $= -3$ dB) is slightly smaller than that for $\gamma = 3$ (i.e., SIR $=$ -4.8 dB) when $\Delta\gamma = 0$. However, with the increase of $\Delta\gamma$, the effect of γ_e on the RMSE of η_1 estimation for $\gamma = 2$ is greater than that for $\gamma = 3$. In other words, the high SIR is more sensitive to $\Delta\gamma$ than the low SIR.

In practical application, if the actual RRCS γ cannot be obtained, a feasible way is to find one $\gamma_e \in [2, 3]$ and ensure that the effect of the estimated γ_e on the RMSE of η_1 estimation is least when γ is equal to either boundary value (i.e., $\gamma = 2$ or $\gamma = 3$). Combining with the conclusion in Fig. 9, research shows that we can select $\gamma_e = 2.1$.To this end, Fig. 10 presented the quantitative analysis results for SNR $= 25$ dB and SIR $= -4$ dB. From Fig. 10, we note that when $\gamma = 2$ or $\gamma = 3$, the differences of the RMSE between the case 2 and case 1 are 0.0171 and 0.0167, respectively. Further, when $\gamma = 2$ or $\gamma = 3$, the differences of the RMSE between the case 3 and case 1 are only 0.0018 and 0.0023 respectively, which can be regarded as some very small errors. It is implicated that we can increase the number of subpulses at distinct frequencies to improve the estimation performance if the actual RRCS is not available.

The method for estimating the RRCS mentioned in the previous paragraph is based on the empirical value. Another feasible method is to estimate the RRCS through GPS/INS. The main idea of this method is illustrated as follows. If the chaff centroid jamming just shapes at the current moment,

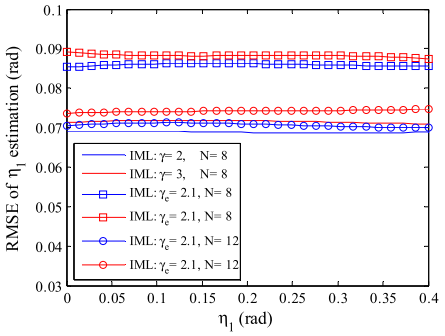

FIGURE 10. RMSE in the estimation of the target's DOA for $\gamma = 2$, $\gamma = 3$ and $\gamma_e = 2.1$. Unmarked lines represent results for the case 1 that actual RRCS γ is known and $N = 8$; □ marked lines represent results for the case 2 that estimated γ_e is 2.1 and $N = 8$; ○ marked lines represent results for the case 3 that estimated γ_e is 2.1 and $N = 12$.

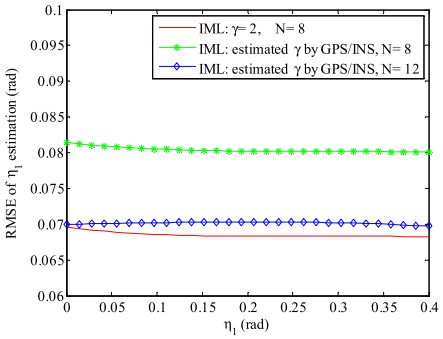

FIGURE 11. Effect of the estimated RRCS by GPS/INS on the RMSE in the estimation of the target's DOA. Unmarked red line represents result that actual RRCS $\gamma = 2$ is known and $N = 8$; * marked green line represents result that estimated γ by GPS/INS and $N = 8$; ⋄ marked blue line represents result that estimated γ by GPS/INS and $N = 12$.

the target azimuth angle with respect to the main beam of the radar seeker at the current moment can be then estimated by utilizing the measured information of GPS/INS, and the detailed process can refer to the literature [2]. To this end, assuming that the DOA of the target obtained by GPS/INS at the current time is $\widehat{\eta}_1$, then, according to (20)∼(22), the estimated RRCS γ_e can be given by

$$\gamma_e = \frac{\left(B_1 - B_2\widehat{\eta}_1\right)^2}{B_2B_0 - B_1^2} \tag{38}$$

It is worth noting that, in the circumstance of chaff centroid jamming, the statistical RCS of vessel and chaff clouds are usually stable (i.e., γ is stable). This assumption is mainly based on two aspects. Firstly, the chaff clouds must expand rapidly since it must present a cross section larger than the vessel, and the disperse time of chaff clouds released by the vessel is usually within a short time (on the order of 10^{-1} s [2]). The average RCS of chaff clouds after diffusion is generally stable [20]. Secondly, for tactical purposes, the vessel commonly goes fast away from the jamming in the adverse direction of wind, and the attitude angle of the vessel changes very small with respect to the main beam of the radar seeker (i.e., the average RCS of the vessel is stable). Therefore, for the anti-ship missile, γ is generally stable when the vessel and jamming are in the same range and angle resolution cells. Under these circumstances, assuming that $\widehat{\eta}_1$ is accurate, the effect of the estimated RRCS by GPS/INS on the RMSE of η_1 estimation is shown in Fig. 11. Similar to Fig. 10, it is also suggested that the estimation performance of η_1 can be improved with the increase of the number of subpulses N, even though SIR and SNR remain fixed. Furthermore, the estimation performance of η_1 in Fig. 11 is comparable to that in Fig. 10, which indicates that the both methods are feasible and effective.

Next, the effect of $\Delta\eta$ (i.e., the separation between the target and jamming) on DOA estimation is studied. The RMSE of η_1 estimation is shown in Fig. 12 for various values of η_1 and $\Delta\eta = 0.4$, 0.6 and 0.8 rad. We set $N = 8$, SNR = 25 dB

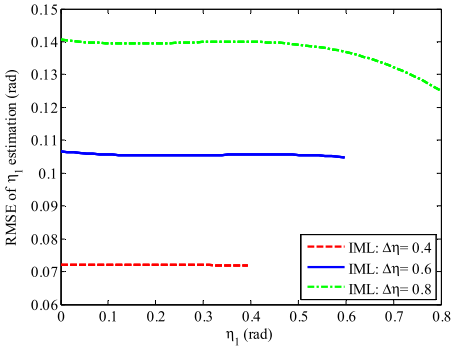

FIGURE 12. Given different $\Delta\eta$, RMSE in the estimation of the target's DOA for SNR = 25 dB, SIR = −4 dB and $N = 8$.

and SIR = −4 dB. It is obviously seen that the RMSE of η_1 estimation decreases with the increase of $\Delta\eta$. However, in the circumstance of chaff centroid jamming, releasing chaff clouds by the vessel downwind and moving upwind is usually the tactical strategy. For radar seeker, the angle between the vessel and jamming (i.e., $\Delta\eta$) is increasing as the time changes. In this case, although the estimation performance of the target' DOA decreases, meanwhile, the accuracy requirement of DOA estimation for tracking is also reduced as the increase of $\Delta\eta$ [9]. It is worth pointing out that, according to the previous conclusion, increasing the number of subpulses at distinct frequencies or enhancing the SNR can improve the decrease of the estimation performance caused by the increase of $\Delta\eta$.

Finally, we compare estimation performance of the proposed methods in this paper with other methods. To compare the performance of different methods for various values of N, SNR and SIR, three data sets are given in the simulation experiments. In the first case, $N = 4$, SNR = 20 dB, SIR = −4.8 dB, are set. In the second, $N = 8$, SNR = 25 dB and SIR= −4 dB are set. In the third situation, $N = 12$, SNR = 30 dB and SIR = −3 dB are given. In the simulation experiment, it is assumed that the RRCS is known. The notation ML, IML and Square root of CRLB are the same as the previous definition. The notation Blair refers to the method

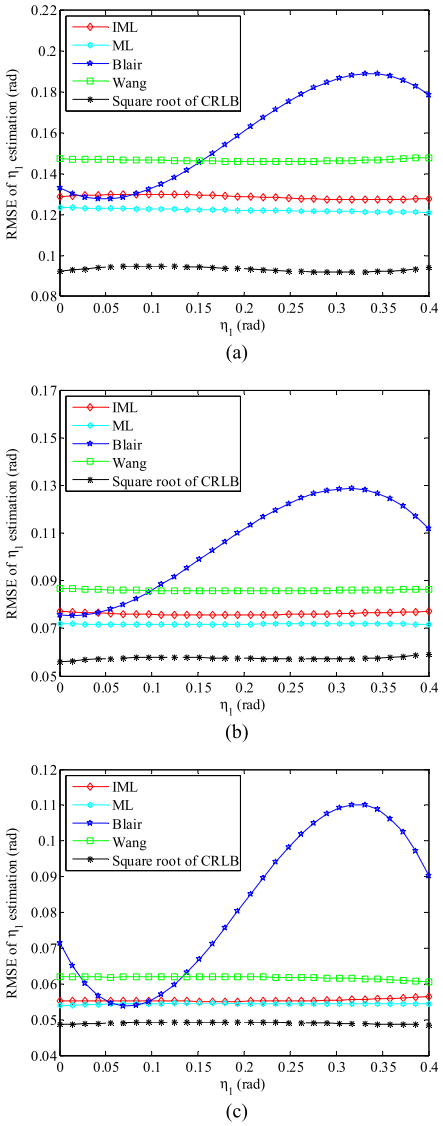

FIGURE 13. Compare the estimation performances of different methods. (a) $N = 4$, SNR = 20 dB and SIR = −4.8 dB; (b) $N = 8$, SNR = 25 dB and SIR = −4 dB; (c) $N = 12$, SNR = 30 dB and SIR = −3 dB.

described in [9], and Wang to the NM2 method presented in [11].

To verify the real-time character of the proposed methods, a test of running time of the program for different methods is presented on a personal computer. For each method, assuming that the echo data has been generated, the program runtime begins with processing the echo data and ends with obtaining the target's DOA. The configuration of the computer has 3.2GHz clock frequency and 16GB random-access memory. 10000 Monte Carlo trials were carried out and the average running time of the program was calculated. In three data sets, the running times (seconds) for the different methods are presented in Table 2. Furthermore, the RMSE comparison of η_1 estimated by different methods is shown in Fig. 13. From Table 2 and Fig. 13, we can draw the following conclusions. Firstly, compared with other methods,

TABLE 2. Comparison of different methods in real-time character.

Methods	First data set	Second data set	Third data set
ML	1.6×10^{-3} s	2.8×10^{-3} s	4.1×10^{-3} s
IML	1.5×10^{-5} s	2.2×10^{-5} s	2.9×10^{-5} s
Blair	9.3×10^{-6} s	9.4×10^{-6} s	9.6×10^{-6} s
Wang	4.7×10^{-6} s	4.7×10^{-6} s	4.8×10^{-6} s

the ML method has a slightly larger computational load, but the estimation accuracy is the best. Secondly, although the estimation performance by the IML is slightly lower than that of the IML, the real-time character of the IML is good than the ML method. Thirdly, the RMSE of η_1 estimated by the Blair methods fluctuates over the range of η_1. And finally, similar to the IML, although the Wang method provides stable estimation performance over the range of η_1, its performance is lower than that of the ML and IML method in conditions of the same SNR, SIR and N. This is because the Wang method is the closed-form solution of the ML function for two unresolved Swerling I targets. However, for two unresolved mixed targets (i.e., Swerling IV and Swerling II targets), it is not optimal compared to the ML and IML method. In addition, the RMSE of η_1 estimated by the proposed methods are more and more close to the square root of the CRLB as the number of subpulses N and SNR increase. In a word, the estimation performance of the proposed methods in this paper is better and more stable that of the other methods. In particular, in practical applications, the ML method or the IML method can be selected according to different requirements of real-time performance and estimation accuracy.

VI. CONCLUSION

In this paper, two alternative methods are proposed to estimate the DOA of the target when the chaff centroid jamming is present. The ML method has high estimation accuracy but large computational load, and the IML method is a compromise between computational load and accuracy. Therefore, in practical applications, if the ML method is satisfies the requirements of real-time performance and estimation accuracy, we select the ML method to estimate the DOA of the target. If not, then we can choose the IML method. In addition, when the actual RRCS is not available, two approaches of estimating RRCS are presented, i.e., estimating the RRCS based on the empirical value and estimating the RRCS by GPS/INS. The first approach is to take a trade-off over the range of RRCS, and the effect of estimated γ_e on the RMSE of η_1 estimation can be restricted least when $\gamma_e = 2.1$ was used. Simulation analysis shows that the two approaches of estimating the RRCS are feasible and effective. Finally, we compared the methods proposed in this paper with the existing methods. Theoretical analyses and simulation experiments indicate that the overall estimation performance of the proposed methods in this paper was better and more stable than that of existing methods. Especially, the performance of the ML and IML

method are more and more close to the square root of the CRLB as the number of subpulses N and SNR increase.

In the circumstance of chaff centroid jamming, the vessel is tracked by the anti-ship missile at first, and then when the vessel realizes the anti-ship missile has been tracking, for self-protection, the vessel will release the chaff centroid jamming. In real application, some factors will affect the accuracy of angle estimate for the radar seeker, such as sea clutter, multipath and target glint. These interesting problems will be further studied in future.

APPENDIX

For two overlapping Swerling IV and Swerling II targets, the function $L_I(\eta_1, \eta_2)$ of η_1 and η_2 is given by

After simplification, the integral (39), as shown at the top of the next page can be rewritten as

where

$$\begin{aligned} R &= \sigma_s^2\sigma_d^2 \\ b_1 &= \sigma_d^2 + \eta_1^2\sigma_s^2 + 4\sigma_s^2\sigma_d^2/a_1^2 \\ b_2 &= \sigma_d^2 + \eta_2^2\sigma_s^2 + \sigma_s^2\sigma_d^2/a_2^2 \\ c_1 &= s_I\sigma_d^2 + \eta_1 d_I\sigma_s^2 \\ c_2 &= s_I\sigma_d^2 + \eta_2 d_I\sigma_s^2 \\ l &= \sigma_d^2 + \eta_1\eta_2\sigma_s^2 \end{aligned} \tag{41}$$

The integral (40), as shown at the top of the next page can be written as a product of two integrals

$$\begin{aligned} L_I(k_1, k_2) = C_0 &\int_{x_2} I_1 \exp\left[-\frac{1}{2R}\left(x_2^2 b_2 - 2x_2 c_2\right)\right] dx_2 \\ &+ C_0 \int_{x_2} I_2 \exp\left[-\frac{1}{2R}\left(x_2^2 b_2 - 2x_2 c_2\right)\right] dx_2 \end{aligned} \tag{42}$$

where

$$\begin{aligned} C_0 &= \frac{4}{(2\pi)^2 a_1^3 a_2 R}\exp\left[-\frac{1}{2R}\left(s_I^2\sigma_d^2 + d_I^2\sigma_s^2\right)\right] \\ I_1 &= \int_{x_1} x_1^2 \exp\left[-\frac{1}{2R}\left(x_1^2 b_1 - 2x_1(c_1 - x_2 l)\right)\right] dx_1 \\ &= \sqrt{\frac{2\pi R}{b_1}}\left(\frac{(c_1 - x_2 l)^2}{b_1^2} + \frac{R}{b_1}\right)\exp\left[\frac{(c_1 - x_2 l)^2}{2Rb_1}\right] \\ I_2 &= \int_{x_1} \frac{a_1^2}{4}\exp\left[-\frac{1}{2R}\left(x_1^2 b_1 - 2x_1(c_1 - x_2 l)\right)\right] dx_1 \\ &= \frac{a_1^2}{4}\sqrt{\frac{2\pi R}{b_1}}\exp\left[\frac{(c_1 - x_2 l)^2}{2Rb_1}\right] \end{aligned} \tag{43}$$

Substituting (43) into (42), then we have

$$\begin{aligned} &L_I(\eta_1, \eta_2) \\ &= = C_0\sqrt{\frac{2\pi R}{b_1}}\exp\left(\frac{c_1^2}{2Rb_1}\right) \\ &\quad\times \int_{x_2}\left(\frac{l^2 x_2^2}{b_1^2} - \frac{2c_1 l x_2}{b_1^2} + \frac{c_1^2}{b_1^2} + \frac{R}{b_1} + \frac{a_1^2}{4}\right) \\ &\quad\times \exp\left[-\frac{1}{2Rb_1}\left(\left(b_1 b_2 - l^2\right)x_2^2 - 2\left(b_1 c_2 - c_1 l\right)x_2\right)\right] dx_2 \end{aligned} \tag{44}$$

Similarly, the function (44) can be written as a product of three integrals

$$L_I(\eta_1, \eta_2) = C_0\sqrt{\frac{2\pi R}{b_1}}\exp\left(\frac{c_1^2}{2Rb_1}\right)(I_3 - I_4 + I_5) \tag{45}$$

where

$$\begin{aligned} I_3 &= \int_{x_2} \frac{l^2 x_2^2}{b_1^2}\exp\left(\frac{\left(l^2 - b_1 b_2\right)x_2^2 + 2\left(b_1 c_2 - c_1 l\right)x_2}{2Rb_1}\right) dx_2 \\ &= \frac{l^2}{b_1^2}\sqrt{\frac{2\pi R b_1}{b_1 b_2 - l^2}}\left[\frac{Rb_1}{b_1 b_2 - l^2} + \frac{(c_2 b_1 - c_1 l)^2}{\left(b_1 b_2 - l^2\right)^2}\right] \\ &\quad\times \exp\left[\frac{(c_2 b_1 - c_1 l)^2}{2Rb_1\left(b_1 b_2 - l^2\right)}\right] \\ I_4 &= \int_{x_2} \frac{2c_1 l x_2}{b_1^2}\exp\left(\frac{\left(l^2 - b_1 b_2\right)x_2^2 + 2\left(b_1 c_2 - c_1 l\right)x_2}{2Rb_1}\right) dx_2 \\ &= \frac{2c_1 l}{b_1^2}\sqrt{\frac{2\pi R b_1}{b_1 b_2 - l^2}}\frac{c_2 b_1 - c_1 l}{b_1 b_2 - l^2}\exp\left[\frac{(c_2 b_1 - c_1 l)^2}{2Rb_1\left(b_1 b_2 - l^2\right)}\right] \\ I_5 &= \int_{x_2}\left(\frac{c_1^2}{b_1^2} + \frac{R}{b_1} + \frac{a_1^2}{4}\right) \\ &\quad\times \exp\left(\frac{\left(l^2 - b_1 b_2\right)x_2^2 + 2\left(b_1 c_2 - c_1 l\right)x_2}{2Rb_1}\right) dx_2 \\ &= \left(\frac{c_1^2}{b_1^2} + \frac{R}{b_1} + \frac{a_1^2}{4}\right)\sqrt{\frac{2\pi R b_1}{b_1 b_2 - l^2}}\exp\left[\frac{(c_2 b_1 - c_1 l)^2}{2Rb_1\left(b_1 b_2 - l^2\right)}\right] \end{aligned} \tag{46}$$

From the above, the function $L_I(k_1, k_2)$ in (39) can be expressed as

$$\begin{aligned} &L_I(\eta_1, \eta_2) \\ &= \frac{4}{2\pi a_1^3 a_2\sqrt{b_1 b_2 - l^2}}\exp\left[-\frac{1}{2R}\left(s_I^2\sigma_d^2 + d_I^2\sigma_s^2\right)\right] \\ &\quad\times \exp\left[\frac{c_1^2 b_2 + c_2^2 b_1 - 2c_1 c_2 l}{2R\left(b_1 b_2 - l^2\right)}\right] \\ &\quad\times \left(f_1^I(\eta_1, \eta_2) + f_2^I(\eta_1, \eta_2)\right) \end{aligned} \tag{47}$$

where

$$\begin{aligned} f_1^I(\eta_1, \eta_2) &= \frac{l^2}{b_1^2}\left(\sigma_{x_2}^2 + \mu_{x_2}^I\right) + \frac{a_1^2}{4} \\ f_2^I(\eta_1, \eta_2) &= \frac{c_1^2}{b_1^2} + \frac{R}{b_1} - \frac{2c_1 l}{b_1}\mu_{x_2}^I \end{aligned} \tag{48}$$

$$\begin{aligned} \sigma_{x_2}^2 &= \frac{Rb_1}{b_1 b_2 - l^2} \\ \mu_{x_2}^I &= \frac{c_2 b_1 - c_1 l}{b_1 b_2 - l^2} \end{aligned} \tag{49}$$

$$L_I(\eta_1,\eta_2)=\int_{x_1}\int_{x_2}\frac{1}{2\pi R}\exp\left(-0.5\left(\begin{bmatrix}s_I-x_1-x_2\\ d_I-\eta_1x_1-\eta_2x_2\end{bmatrix}^{\mathrm{T}}\begin{bmatrix}\sigma_s^2 & 0\\ 0 & \sigma_d^2\end{bmatrix}\begin{bmatrix}s_I-x_1-x_2\\ d_I-\eta_1x_1-\eta_2x_2\end{bmatrix}\right)\right)\times\frac{4}{\sqrt{2\pi}a_1^3}\left(x_1^2+\frac{a_1^2}{4}\right)\exp\left(-\frac{2x_1}{a_1^2}\right)\frac{1}{\sqrt{2\pi a_2^2}}\exp\left(-\frac{x_2}{2a_2^2}\right)dx_1dx_2 \quad (39)$$

$$L_I(\eta_1,\eta_2)=\frac{4}{(2\pi)^2a_1^3a_2R}\exp\left[-\frac{1}{2R}\left(s_I^2\sigma_d^2+d_I^2\sigma_s^2\right)\right]\times\int_{x_1}\int_{x_2}\exp\left[-\frac{1}{2R}\left(x_1^2b_1+x_2^2b_2-2x_1\left(c_1-x_2l\right)-2x_2c_2\right)\right]\left(x_1^2+\frac{a_1^2}{4}\right)dx_1dx_2 \quad (40)$$

Similar to the previous derivation, we can also obtain the function $L_Q(\eta_1,\eta_2)$

$$\begin{aligned}L_Q(\eta_1,\eta_2)&=\frac{4}{2\pi a_1^3a_2\sqrt{b_1b_2-l^2}}\exp\left[-\frac{1}{2R}\left(s_Q^2\sigma_d^2+d_Q^2\sigma_s^2\right)\right]\\&\times\exp\left[\frac{d_1^2b_2+d_2^2b_1-2d_1d_2l}{2R\left(b_1b_2-l^2\right)}\right]\\&\times\left(f_1^Q(\eta_1,\eta_2)+f_2^Q(\eta_1,\eta_2)\right)\end{aligned} \quad (50)$$

where

$$\begin{aligned}d_1&=s_Q\sigma_d^2+\eta_1d_Q\sigma_s^2\\d_2&=s_Q\sigma_d^2+\eta_2d_Q\sigma_s^2\end{aligned} \quad (51)$$

$$f_1^Q(\eta_1,\eta_2)=\frac{l^2}{b_1^2}\left(\sigma_{x_2}^2+\mu_{x_2}^Q\right)+\frac{a_1^2}{4}$$

$$f_2^Q(\eta_1,\eta_2)=\frac{c_1^2}{b_1^2}+\frac{R}{b_1}-\frac{2c_1l}{b_1}\mu_{x_2}^Q \quad (52)$$

$$\mu_{x_2}^Q=\frac{d_2b_1-d_1l}{b_1b_2-l^2} \quad (53)$$

REFERENCES

[1] D. C. Schleher, *Electronic Warfare in the Information Age*. Norwood, MA, USA: Artech House, 1999.

[2] Y. Yang, D.-J. Feng, W.-M. Zhang, X.-S. Wang, and S.-P. Xiao, "Detection of chaff centroid jamming aided by GPS/INS," *IET Radar Sonar Navigat.*, vol. 7, no. 2, pp. 130–142, Feb. 2013.

[3] Y. Yang, S.-P. Xiao, D.-J. Feng, and X.-S. Wang, "Polarisation oblique projection for radar seeker tracking in chaff centroid jamming environment without prior knowledge," *IET Radar Sonar Navigat.*, vol. 8, no. 9, pp. 1195–1202, Sep. 2014.

[4] S.-P. Lee, B.-L. Cho, S.-M. Lee, J.-E. Kim, and Y.-S. Kim, "Unambiguous angle estimation of unresolved targets in monopulse radar," *IEEE Trans. Aerosp. Electron. Syst.*, vol. 51, no. 2, pp. 1170–1177, Apr. 2015.

[5] S. M. Sherman, "Complex indicated angles applied to unresolved radar targets and multipath," *IEEE Trans. Aerosp. Electron. Syst.*, vol. AES-7, no. 1, pp. 160–170, Jan. 1971.

[6] Y. Zheng, S.-M. Tseng, and K.-B. Yu, "Closed-form four-channel monopulse two-target resolution," *IEEE Trans. Aerosp. Electron. Syst.*, vol. 39, no. 3, pp. 1083–1089, Jul. 2003.

[7] D. F. Crouse, U. Nickel, and P. Willett, "Comments on 'closed-form four-channel monopulse two-target resolution'," *IEEE Trans. Aerosp. Electron. Syst.*, vol. 48, no. 1, pp. 913–916, Jan. 2012.

[8] F. Vincent, O. Besson, and E. Chaumette, "Approximate unconditional maximum likelihood direction of arrival estimation for two closely spaced targets," *IEEE Signal Process. Lett.*, vol. 22, no. 1, pp. 86–89, Jan. 2014.

[9] W. D. Blair and M. Brandt-Pearce, "Monopulse DOA estimation of two unresolved Rayleigh targets," *IEEE Trans. Aerosp. Electron. Syst.*, vol. 37, no. 2, pp. 452–469, Apr. 2001.

[10] A. Sinha, T. Kirubarajan, and Y. Bar-Shalom, "Maximum likelihood angle extractor for two closely spaced targets," *IEEE Trans. Aerosp. Electron. Syst.*, vol. 38, no. 1, pp. 183–203, Jan. 2002.

[11] Z. Wang, A. Sinha, P. Willett, and Y. Bar-Shalom, "Angle estimation for two unresolved targets with monopulse radar," *IEEE Trans. Aerosp. Electron. Syst.*, vol. 40, no. 3, pp. 998–1019, Jul. 2004.

[12] X. Zhang, P. Willett, and Y. Bar-Shalom, "Detection and localization of multiple unresolved extended targets via monopulse radar signal processing," *IEEE Trans. Aerosp. Electron. Syst.*, vol. 45, no. 2, pp. 455–472, Apr. 2005.

[13] Y. Zhang, Q.-F. Liu, R.-J. Hong, P.-P. Pan, and Z.-M. Deng, "A novel monopulse angle estimation method for wideband LFM radars," *Sensors*, vol. 16, no. 6, p. 817, Oct. 2016.

[14] J. Ma, L. Shi, Y. Li, S. Xiao, and X. Wang, "Angle estimation of extended targets in main-lobe interference with polarization filtering," *IEEE Trans. Aerosp. Electron. Syst.*, vol. 53, no. 1, pp. 169–189, Feb. 2017.

[15] S. J. Asseo, "Detection of target multiplicity using monopulse quadrature angle," *IEEE Trans. Aerosp. Electron. Syst.*, vol. AES-17, no. 2, pp. 271–280, Mar. 1981.

[16] W. D. Blair and M. Brandt-Pierce, "Statistical description of monopulse parameters for tracking Rayleigh targets," *IEEE Trans. Aerosp. Electron. Syst.*, vol. 34, no. 2, pp. 597–611, Mar. 1997.

[17] T. Shores, *Applied Linear Algebra and Matrix Analysis*. Berlin, Germany: Springer, 2007.

[18] M. Long, *Radar Reflectivity of Land and Sea*, 3rd ed. Norwood, MA, USA: Artech House, 2001.

[19] Y. Yang, S.-P. Xiao, D.-J. Feng, and W.-M. Zhang, "Modelling and simulation of spatial-temporal correlated K distributed clutter for coherent radar seeker," *IET Radar Sonar Navigat.*, vol. 8, no. 1, pp. 1–8, Jan. 2014.

[20] D. W. Seo, H. J. Nam, O. J. Kwon, and N. H. Myung, "Dynamic RCS estimation of chaff clouds," *IEEE Trans. Aerosp. Electron. Syst.*, vol. 48, no. 3, pp. 2114–2127, Jul. 2012.

YEMIN LIU was born in Yongzhou, Hunan, China, in 1982. He received the M.S. degree in information and communication engineering from the National University of Defense Technology, Changsha, China, in 2010, where he is currently pursuing the Ph.D. degree. His fields of interest include electronic countermeasures and polarimetric radar information processing.

SHIQI XING was born in Jiujiang, China, in 1984. He received the Ph.D. degree in information and communication engineering from the National University of Defense Technology, Changsha, China, in 2013. His research interests include polarimetric synthetic aperture radar (SAR) data calibration, SAR tomography, interferometric SAR signal processing, and electronic countermeasures.

YONGCAI LIU was born in Harbin, China, in 1988. He received the M.S. and Ph.D. degrees in information and communication engineering from the National University of Defense Technology, Changsha, China, in 2013 and 2017, respectively. His fields of interest include synthetic aperture radar imaging and electronic countermeasures.

YONGZHEN LI was born in 1977. He received the B.E. and Ph.D. degrees from the School of Electronic Science, National University of Defense Technology, Changsha, Hunan, China, in 1999 and 2004, respectively. He is currently a Professor with the National University of Defense Technology. His current research interests include signal processing, radar polarimetry, and target recognition.

XUESONG WANG was born in 1972. He received the B.E. and Ph.D. degrees from the School of Electronic Science, National University of Defense Technology, Changsha, Hunan, China, in 1994 and 1999, respectively. He is currently a Professor with the National University of Defense Technology. His current research interests include polarimetric radar information processing and target recognition. He is a fellow of CIE.